Shock formation processes in colliding two collisionless plasmas in a magnetic field

Koji Yamauchi and Yukiharu Ohsawa[a)]
Department of Physics, Nagoya University, Nagoya 464-8602, Japan

(Received 11 December 2006; accepted 2 April 2007; published online 18 May 2007)

Interactions of exploding and surrounding plasmas are analyzed with theory and particle simulations for the case in which the initial velocity $\boldsymbol{v}_0$ of the exploding plasma is perpendicular to the weak external magnetic field $\boldsymbol{B}_0$; because of the fast $\boldsymbol{v}_0$ and weak $\boldsymbol{B}_0$, the gyroradius v_0/Ω_i is much longer than shock widths. After the penetration of the exploding ions, the electric field induced by the cross-field plasma motion quickly accelerates the surrounding ions in the direction perpendicular to $\boldsymbol{v}_0$ and $\boldsymbol{B}_0$. Owing to the magnetic force, however, the surrounding ions that were once overtaken by the exploding ions can pass them later. Because the electron guiding centers move with the $\boldsymbol{E}\times\boldsymbol{B}$ drift, the two kinds of electrons are not mixed. Further, because of the deceleration of the exploding ions in the front layer, the plasma density and magnetic-field strength go up there. This field reflects the surrounding ions forward and exploding ions backward. This generates two large pulses, which then develop into forward and reverse shock waves. Up to the generation of the two pulses, the time and length scales are basically determined by v_0 and B_0. © *2007 American Institute of Physics*. [DOI: 10.1063/1.2734580]

I. INTRODUCTION

Shock waves can be generated from strong disturbances, such as laser implosions, solar flares, and supernova explosions, and play a crucial role in the development of the system; see Refs. 1–5, and references therein. They have been studied, therefore, by many authors from various points of view; for instance, nonlinear wave propagation, energy transport, particle acceleration, and evolution of supernova remnants; see Refs. 6–11, and references therein. Further, laboratory experiments of shock waves with use of intense lasers have recently started to model astrophysical phenomena, such as supernovae.[12]

In a collisional fluid, the local velocity distribution function of particles should be nearly Maxwellian even after a strong disturbance has been generated. The time in which a shock wave is formed may be estimated from the characteristic curves of the fluid.[6]

Shock formation processes in collisionless plasmas would be quite different from those in collisional fluids. In a collisionless plasma, ion and electron velocity distribution functions can be far from Maxwellian for long periods of time. Therefore, if an explosion occurs in a plasma without external magnetic fields, the exploding plasma could penetrate deep into the surrounding plasma. The two plasmas having different fluid velocities can overlap in a wide area, which will not occur in collisional fluids. Some kinds of two-stream instabilities may then play some role in relaxation and shock formation processes.[13] Spitzer suggested,[14] however, that if there is an external magnetic field, it would affect the plasma evolution and shock formation.

In the present paper, we study the interaction between exploding and surrounding plasmas and resultant formation processes of shock waves in an external magnetic field. We are particularly interested in the case in which the field is so weak that the ion gyroradius is much greater than the shock width.

The gyroradii can be considerably larger or smaller than the shock width, depending on the plasma density, speed, and magnetic-field strength B. Roughly speaking, the width of the shock transition region is independent of B and is proportional to $n_e^{-1/2}$, where n_e is the plasma (electron) density; it is $\sim c/\omega_{pe}$ (electron skin depth) for quasiperpendicular shock waves and $\sim c/\omega_{pi}$ (ion inertia length) for oblique shocks; for a more precise discussion on the shock width, see, for instance, Refs. 15–19. For a plasma density $n_e=1\ \mathrm{cm}^{-3}$, their lengths are $c/\omega_{pe}=5.3\times10^5$ cm and $c/\omega_{pi}=2.3\times10^7$ cm. The gyroradius is proportional to v_0/B, where v_0 is the particle speed. Hence, it can be smaller than c/ω_{pi} in strong magnetic fields. For instance, if a plasma moves with a speed $v_0=10^9\ \mathrm{cm\ s}^{-1}$ in an external magnetic field with $B=1$ G, the ion (hydrogen) gyroradius is $\rho_{i0}=1.0\times10^5$ cm, which is $\sim1/200$ of the above c/ω_{pi}. In weak magnetic fields, ρ_{i0} can be much greater than c/ω_{pi}; we study such cases in this paper. For a magnetic field such that $B=10^{-6}$ G, which is a typical strength of interstellar magnetic fields, the ion gyroradius is $\rho_{i0}=1.0\times10^{11}$ cm, which is ~4000 times as large as the c/ω_{pi}. (The gyroradii for thermal speeds are shorter than these in many cases. We have taken large v_0 because we are interested in high fluid velocities.)

In Sec. II, we analyze the motions of exploding and surrounding particles for a case in which the initial velocity of the exploding plasma, which is taken to be $\boldsymbol{v}_0=(v_0,0,0)$, is perpendicular to the external magnetic field $\boldsymbol{B}_0=(0,0,B_{z0})$ while the surrounding plasma is at rest; these two semi-infinite plasmas initially have a plane common boundary. The cross-field motion of the exploding ions induces electric

[a)]Electronic mail: ohsawa@nagoya-u.jp

field E_y perpendicular to both $\boldsymbol{v}_0$ and $\boldsymbol{B}_0$. In the region where the exploding ions have penetrated, this electric field accelerates the surrounding ions in the y direction; v_y is then converted to v_x by the $\boldsymbol{v}\times\boldsymbol{B}$ force. In addition, v_x of the exploding ions is converted to v_y. As a result, the surrounding ions that have been overtaken once by the exploding ions can pass them later. Electron guiding centers move with the $\boldsymbol{E}\times\boldsymbol{B}$ drift; thus, the exploding electrons are always behind the surrounding electrons.

In Sec. III, we use a one-dimensional (one space coordinate and three velocities), relativistic, electromagnetic particle simulation code to study these processes. To observe the evolution of moving long plasmas, we take a large grid size of 16 384. It is found that the trajectories of exploding and surrounding particles support the above theoretical predictions, penetration and deceleration of the front part of the exploding ions, and overtaking of the surrounding ions. Figures of phase spaces and field profiles show that immediately after the penetration of the exploding ions, the acceleration of the surrounding ions in the y direction begins; these velocities are then quickly converted to v_x, which leads to the overtaking. Furthermore, around the time when the flow velocity v_x of the exploding ions has sufficiently decreased in the front layer, collective effects become important. The plasma density increases, and the magnetic field becomes strong there. The intensified magnetic field in the front layer reflects the surrounding ions forward and the exploding ions backward, which generates two large pulses. This time is of the order of the ion gyroperiod, $\Omega_i t\sim 1$. The two pulses develop into shock waves, one going forward and the other backward. (We do not expect that these pulses satisfy the Rankine-Hugoniot relations. These pulses are in a collisionless plasma; as stated above, the velocity distribution functions near the pulses can deviate considerably from Maxwellians. In either ion-acoustic waves or magnetosonic waves, we know soliton solutions. In collisionless plasmas, the symmetry of these soliton solutions can be destroyed by, for instance, particle reflection from the wave front, particle trapping, and instabilities. These waves with nonsymmetric profiles are commonly called shock waves.[20–23] In the present paper, we also call nonsymmetric large-amplitude magnetosonic pulses the shock waves.)

We summarize our work in Sec. IV.

II. CONSIDERATIONS ON PLASMA MOTIONS

We consider a situation in which two plasmas exist separately at $t=0$ in an external magnetic field $\boldsymbol{B}_0=(0,0,B_{z0})$. As shown in Fig. 1, one is in the region $x\leqslant b$ having an ion density n_{iE0} and a high fluid-speed $v_0(>0)$ in the positive x direction, and the other is in the region $x>b$ with a density n_{iS0} at rest. The former can be viewed as an exploding plasma while the latter is a surrounding plasma. The speed v_0 is supposed to be much higher than the Alfvén speed v_A and the ion thermal velocity $v_{Ti}=(T_i/m_i)^{1/2}$, where T_i is the ion temperature. Hence, the ion gyroradius $\rho_{i0}=v_0/\Omega_i$, where Ω_i is the gyrofrequency $\Omega_i=q_iB_z/(m_ic)$, is much greater than the ion inertia length c/ω_{pi} and the thermal gyroradius $\rho_{i\mathrm{T}}=v_{Ti}/\Omega_i$.

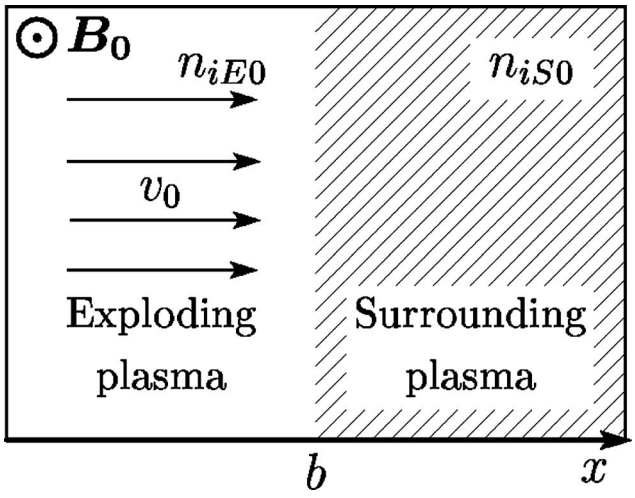

FIG. 1. Exploding and surrounding plasmas at $t=0$. The exploding plasma exists in the region $x<b$ with a velocity v_0.

In addition, the ion gyroradius ρ_{i0} is m_i/m_e times as large as that of electrons for the same speed, $\rho_{e0}=v_0/|\Omega_e|$. After the penetration of the exploding plasma in the surrounding plasma, therefore, the behavior of the electrons should be quite different from that of the ions. For the length scale

$$\rho_{e0}<|x-b|\lesssim\rho_{i0}, \tag{1}$$

and for the time scale

$$|\Omega_e|^{-1}<t\lesssim|\Omega_i|^{-1}, \tag{2}$$

we can treat the electrons as strongly magnetized particles. The drift approximation will therefore be applicable to the electrons, whereas it is not valid for the ions. We are concerned with plasma behavior in the length scale (1) and time scale (2) after the penetration.

A. Characteristics of ions and electrons

The two plasmas can overlap in some region in the coordinate space. Their evolution can be described by the Vlasov equation. For the ions, it reads

$$\frac{\partial f}{\partial t}+\boldsymbol{v}\cdot\frac{\partial f}{\partial \boldsymbol{x}}+\frac{q_i}{m_i}\left(\boldsymbol{E}+\frac{\boldsymbol{v}\times\boldsymbol{B}}{c}\right)\cdot\frac{\partial f}{\partial \boldsymbol{v}}=0. \tag{3}$$

The distribution function f is constant along the characteristics,

$$\frac{d\boldsymbol{x}}{dt}=\boldsymbol{v}, \tag{4}$$

$$\frac{d\boldsymbol{v}}{dt}=\frac{q_i}{m_i}\left(\boldsymbol{E}+\frac{\boldsymbol{v}\times\boldsymbol{B}}{c}\right). \tag{5}$$

If the two plasmas are cold, we may write the distribution function of the exploding ions as

$$f_E(\boldsymbol{x},\boldsymbol{v},t)=n_{iE}(x,t)\,\delta[\boldsymbol{v}-\boldsymbol{v}_{iE}(x,t)], \tag{6}$$

and that of the surrounding ions as

$$f_S(\boldsymbol{x},\boldsymbol{v},t) = n_{iS}(x,t)\,\delta[\boldsymbol{v} - \boldsymbol{v}_{iS}(x,t)], \tag{7}$$

with $f=f_E+f_S$.

Firsty, we discuss exploding ions. As in perpendicular shock waves, we assume that $E_z=0$ and that the magnetic field has only a z component. Then, the equation for $\boldsymbol{v}_{iE}(x,t)$ would become

$$m_i\frac{dv_{ixE}}{dt} = q_iE_x + q_i\frac{v_{iyE}B_z}{c}, \tag{8}$$

$$m_i\frac{dv_{iyE}}{dt} = q_iE_y - q_i\frac{v_{ixE}B_z}{c}. \tag{9}$$

The momentum in the z direction is constant. For one-dimensional disturbances, $\partial/\partial y=\partial/\partial z=0$, the time derivative in Eqs. (8) and (9) is defined as

$$\frac{d}{dt} = \frac{\partial}{\partial t} + v_{ixE}\frac{\partial}{\partial x}. \tag{10}$$

We assume the following ordering:

$$E_y \sim \left|\frac{\boldsymbol{v}_{iE}\times\boldsymbol{B}}{c}\right| \gg E_x. \tag{11}$$

Strong E_y is generated because of the cross-field plasma motion. Since E_x is the longitudinal electric field, the fact that E_x is weak is a result of charge neutrality, which holds in low-frequency magnetohydrodynamic phenomena. The field E_x could become strong only in the vicinity of the front of the exploding plasma. We therefore ignore E_x in the zeroth-order analysis for the exploding plasma. [Relation (11) is an ordering. It does not claim that the ions move with the $\boldsymbol{E}\times\boldsymbol{B}$ drift.]

Then, for spatially uniform fields, we obtain solutions

$$v_{ixE} = v_d + v_\perp\cos(-\Omega_it+\delta), \tag{12}$$

$$v_{iyE} = v_\perp\sin(-\Omega_it+\delta), \tag{13}$$

where $v_\perp$ is taken to be positive, and v_d is given by

$$v_d = \frac{cE_y}{B_z}. \tag{14}$$

Under the initial conditions that $v_{ixE}=v_0(>0)$ and $v_{iyE}=0$, the initial phase δ becomes zero, and

$$v_0 = v_d + v_\perp. \tag{15}$$

Hence, the initial ion speed is greater than the drift speed, $v_0>v_d$.

If v_0 is equal to v_d, then $v_\perp=0$; hence, $v_{ixE}(t)=v_0$ and $v_{iyE}(t)=0$. This represents an equilibrium plasma flow in the x direction due to the $\boldsymbol{E}\times\boldsymbol{B}$ drift; i.e., all the ions and electrons move with the drift speed (14). We note that the electric energy generated in association with the cross-field plasma motion is much smaller than the kinetic energy,

$$\frac{E_y^2/(8\pi)}{n_{iE0}m_iv_0^2/2} = \frac{v_d^2}{v_0^2}\frac{v_A^2}{c^2} \ll 1, \tag{16}$$

where the Alfvén speed is supposed to be much smaller than the speed of light. This implies that if we suddenly give a high initial speed v_0 to a plasma in the entire region, this system would quickly reach an equilibrium state, generating E_y without losing much kinetic energy. In this case, substituting the relation $v_d\simeq v_0$ in Eq. (14), we find the field strength as

$$E_y \simeq \frac{v_0}{c}B_{z0}. \tag{17}$$

In the region where the exploding and surrounding ions coexist, however, this does not hold, and v_0 is not equal to v_d.

The characteristic curves in the coordinate space corresponding to Eqs. (12) and (13) with $\delta=0$ are given as

$$x_{iE} = v_dt - \frac{v_\perp}{\Omega_i}\sin(-\Omega_it) + x_{E0}, \tag{18}$$

$$y_{iE} = -\frac{v_\perp}{\Omega_i}[1-\cos(-\Omega_it)] + y_{E0}, \tag{19}$$

where (x_{E0},y_{E0}) is the initial position; $x_{E0}\leqslant b$. We denote the x position of an exploding ion that is initially at the boundary, $x_{E0}=b$, by $x_{iEb}(t)$. Equation (12) indicates that v_{ixE} becomes zero at

$$\Omega_it = \arccos(-v_d/v_\perp). \tag{20}$$

If $v_d/v_\perp\geqslant 1$, the velocity v_{ixE} would not change sign, and x_{iE} would monotonically increase.

We use the drift approximation for the motions of the exploding and surrounding electrons,

$$v_{ex} = v_d. \tag{21}$$

Consequently, the two kinds of electrons, which are initially separated in the coordinate space, will not be mixed up later. This boundary is denoted by $x_{eb}(t)$; hence, $x_{eb}(0)=b$.

Next, we consider the surrounding ions. Because $\boldsymbol{v}_{iS}(0)=0$, the $\boldsymbol{v}\times\boldsymbol{B}$ force is small in the early phase. We therefore include the effect of E_x as well as E_y. However, we still use the assumption that the electric field ratio $r_{xy}=E_x/E_y$ is small,

$$|r_{xy}| = |E_x/E_y| \ll 1. \tag{22}$$

We suppose that the front of the exploding ions, $x_{iEb}(t)$, passes a position x_{S0} at t_S for the first time,

$$x_{S0} = x_{iEb}(t_S) = v_dt_S - (v_\perp/\Omega_i)\sin(-\Omega_it_S) + b. \tag{23}$$

For $\Omega_it\ll 1$, t_S is approximately given as $t_S=(x_{S0}-b)/v_0$. Then, on account of Eq. (22), we find from the equation of motion that

$$v_{ixS}(x_{S0},t) = v_d[1-(1+r_{xy}^2/2)\cos(-\Omega_it'-r_{xy})], \tag{24}$$

$$v_{iyS}(x_{S0},t) = -cE_x/B - v_d(1+r_{xy}^2/2)\sin(-\Omega_it'-r_{xy}), \tag{25}$$

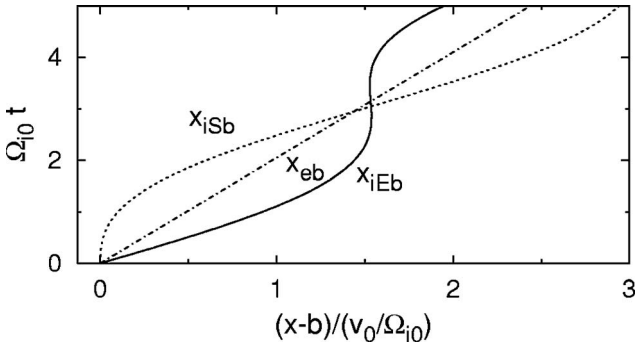

FIG. 2. Theoretical trajectories of x_{iEb}, x_{iSb}, and x_{eb}.

$$x_{iS}(x_{S0},t) = v_d t' + \frac{v_d}{\Omega_i}\left(1 + \frac{r_{xy}^2}{2}\right)\sin(-\Omega_i t' - r_{xy}) + x_{S0} + \frac{v_d}{\Omega_i} r_{xy}, \tag{26}$$

where $t' = t - t_S(x_{S0})$. The speed of the surrounding ions is small in the early phase. However, it becomes comparable to v_d later.

If we ignore the $\boldsymbol{v}\times\boldsymbol{B}$ force in the equation of motion, we obtain

$$v_{ixS}(x_{S0},t) = (q_i/m_i)E_x t', \tag{27}$$

$$v_{iyS}(x_{S0},t) = (q_i/m_i)E_y t', \tag{28}$$

$$x_{iS}(x_{S0},t) = [q_i/(2m_i)]E_x t'^2 + x_{S0}. \tag{29}$$

These equations suggest that the motion v_{ixS} would act to suppress the longitudinal electric field E_x. Because of the transverse electric field E_y ($\gg E_x$), v_{iyS} quickly increases after the penetration of the exploding ions. Using Eq. (28), we can rewrite the inequality $q_i v_{iyS} B/c < q_i E_x$ as

$$\Omega_i t' < r_{xy}. \tag{30}$$

Indeed, Eqs. (24)–(26) reduce to Eqs. (27)–(29), respectively, under the condition (30).

Figure 2 shows the trajectories of particles that are initially at the boundary $x=b$: x_{iEb} for exploding ions, x_{iSb} for surrounding ions, and x_{eb} for electrons, which we have drawn with the aid of Eqs. (18), (21), and (26). Here, the input parameters are $v_0/c=0.5$, $E_y/B_{z0}=0.25$, and $r_{xy}=0.1$. (We have chosen these values so that we can compare Fig. 2 with the simulation results in Sec. III.) The following relation holds in the early phase:

$$x_{iSb}(t) < x_{eb}(t) < x_{iEb}(t), \tag{31}$$

because $v_{ixS} < v_d < v_0$ for $\Omega_i t \ll 1$. In the region $x_{eb} < x < x_{iEb}$, which will be called the front layer, there exist three kinds of particles; surrounding ions and electrons and exploding ions. In the region $x_{iSb} < x < x_{eb}$, there exist exploding ions and electrons and surrounding ions.

The two characteristic curves $x_{iEb}(t)$ and $x_{iSb}(t)$ meet again later. We can obtain this time from Eqs. (18) and (26). Since the field strengths at $x_{iEb}(t)$ and $x_{iSb}(t)$ may be different (see Secs. II B and III), we denote the gyrofrequency at $x_{iEb}(t)$ by Ω_{iE} and that at $x_{iSb}(t)$ by Ω_{iS}. We then have

$$-\frac{v_\perp}{\Omega_{iE}}\sin(-\Omega_{iE}t) = -\frac{v_d}{\Omega_{iS}}\left(1 + \frac{r_{xy}^2}{2}\right)\sin(-\Omega_{iS}t + r_{xy}) + \frac{v_d}{\Omega_{iS}} r_{xy}. \tag{32}$$

Because r_{xy} is small, this becomes

$$-\frac{v_\perp}{\Omega_{iE}}\sin(-\Omega_{iE}t) = \frac{v_d}{\Omega_{iS}}[\sin(-\Omega_{iS}t) - r_{xy}\cos(-\Omega_{iS}t)] + \frac{v_d}{\Omega_{iS}} r_{xy}, \tag{33}$$

where the terms up to r_{xy}^2 were retained. In the case in which $\Omega_{iE}=\Omega_{iS}(=\Omega_i)$, this can be further reduced to

$$\tan\left(-\frac{\Omega_i t}{2}\right) = -\frac{v_d + v_\perp}{r_{xy} v_d}. \tag{34}$$

Since the right-hand side gives a large value in magnitude, we see that

$$\Omega_i t \sim \pi. \tag{35}$$

When $\Omega_{iE} \neq \Omega_{iS}$ and $r_{xy} \ll 1$, from Eq. (33) we have a rough estimate,

$$-\frac{v_\perp}{\Omega_{iE}}\sin(-\Omega_{iE}t) = \frac{v_d}{\Omega_{iS}}\sin(-\Omega_{iS}t). \tag{36}$$

If $v_\perp/\Omega_{iE} \ll v_d/\Omega_{iS}$, we obtain $\Omega_{iS}t \sim \pi$.

B. Collective effects

The electrons that exist in the front layer, $x_{eb} < x < x_{iEb}$, at time t were in the region $b < x < x_{iEb}(t)$ initially. We therefore have the following relation:

$$\int_{x_{eb}(t)}^{x_{iEb}(t)} n_{eS}(x,t)dx = n_{eS0}[x_{iEb}(t) - b], \tag{37}$$

where n_{eS0} is the initial density of the surrounding electrons. Let $\langle n_{eS}\rangle$ designate the electron density averaged over x in this layer. Then, we obtain

$$\frac{\langle n_{eS}\rangle}{n_{eS0}} = \frac{x_{iEb}(t) - b}{x_{iEb}(t) - x_{eb}(t)}. \tag{38}$$

Using the charge neutrality condition, $n_{iE}+n_{iS}=n_{eS}$, we find the width of the front layer as

$$x_{iEb}(t) - x_{eb}(t) = \frac{n_{eS0}}{\langle n_{iE} + n_{iS}\rangle}[x_{iEb}(t) - b]. \tag{39}$$

As n_{iE} increases, the coefficient $n_{eS0}/\langle n_{iE}+n_{iS}\rangle$ should decrease. The width $(x_{iEb}-x_{eb})$ should therefore be smaller when the density of the exploding plasma is high, $n_{iE} \gg n_{eS0}$, than when $n_{iE} \sim n_{eS0}$. This will be quantitatively examined with simulations below in Fig. 12 in Sec. III B.

Magnetic-field lines, as well as the plasma, should be compressed in this layer, because the field lines are frozen in

the electron fluid. In fact, because the electrons move with the $\boldsymbol{E}\times\boldsymbol{B}$ drift, we can put the z component of Faraday's law into the following form:

$$\frac{\partial B_z}{\partial t}+\frac{\partial}{\partial x}(v_{ex}B_z)=0. \tag{40}$$

We have the continuity equation for the electrons if we replace B_z by n_e. The electron density n_e is governed by the same equation as B_z.

Further, Eq. (37) indicates that the plasma density in the front layer should become quite high around the time given by (34), when x_{iEb} and x_{eb} are close. The magnetic field should also become strong there. As will be shown in Sec. III with simulations, this has significant effects on plasma behavior.

III. SIMULATIONS OF PLASMA COLLISION

A. Simulation model

We now use a one-dimensional (one space coordinate and three velocities), relativistic, electromagnetic particle simulation code with full ion and electron dynamics[24] to study the penetration of an exploding plasma in a surrounding plasma and resultant formation of shock waves.

At $t=0$, we have an exploding plasma with a fluid velocity $\boldsymbol{v}_0=(v_0,0,0)$ in the region $x<b$ and a surrounding plasma at rest in the region $x>b$ in a uniform external magnetic field $\boldsymbol{B}_0=(0,0,B_{z0})$. Their initial densities are chosen to be $n_{iE0}=2n_{iS0}$. Because $q_i=-q_e$ in the simulations, the initial ion and electron densities are the same; $n_{iE0}=n_{eE0}$ and $n_{iS0}=n_{eS0}$. To observe the long-time evolution of the two plasmas, we take a large system size $L=16384\Delta_g$, where Δ_g is the grid spacing. The numbers of simulation particles are $N_i=N_e\simeq 1.05\times 10^6$. Other simulation parameters are as follows. The ion-to-electron mass ratio is $m_i/m_e=100$. The speed of light is $c/(\omega_{pe}\Delta_g)=4$, where ω_{pe} is the electron plasma frequency calculated with use of the density averaged over the entire plasma region. The magnetic field strength is $|\Omega_e|/\omega_{pe}=0.1$; hence the Alfvén speed is $v_A/(\omega_{pe}\Delta_g)=0.04$. The thermal speeds are $v_{Ti}/(\omega_{pe}\Delta_g)=0.1$ and $v_{Te}/(\omega_{pe}\Delta_g)=1.0$; the sound speed is $c_s/(\omega_{pe}\Delta_g)=0.18$ for the specific-heat ratio $\gamma_e=\gamma_i=5/3$. The speed of the linear magnetosonic wave is $v_{\rm ms}/(\omega_{pe}\Delta_g)=0.18$, where $v_{\rm ms}$ is defined by $v_{\rm ms}=(v_A^2+c_s^2)^{1/2}$. The time step is $\omega_{pe}\Delta t=0.05$.

B. Simulation results

Figure 3 displays the trajectories of exploding ions (top panel), surrounding ions (middle panel), and electrons (bottom panel). For comparison, we have drawn the trajectories of x_{iEb} (thick solid lines) and x_{iSb} (thick dotted lines) in all the panels. Here, the initial speed of the exploding ions is $v_0/(\omega_{pe}\Delta_g)=2.05$. Inspection of the top and middle panels shows that the surrounding ions begin to move upon the passage the exploding ions. We see that x_{iEb} moves faster than x_{iSb} in the early phase. However, x_{iSb} is soon accelerated and passes $x_{iEb}(t)$ at $\Omega_{i0}t=2.1$ ($\omega_{pe}t=2100$), where Ω_{i0} is the ion gyrofrequency calculated with use of the external magnetic field strength. This time is consistent with the order

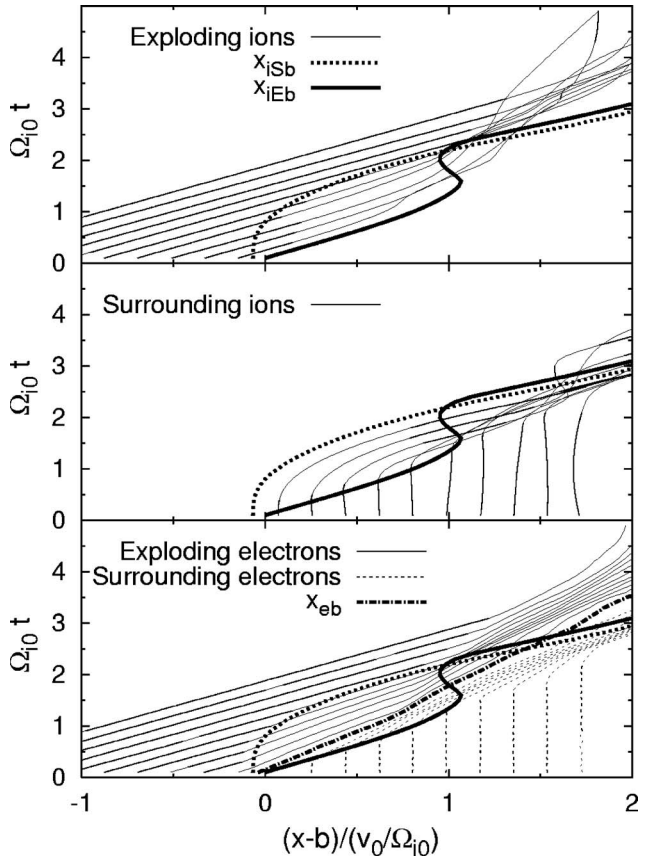

FIG. 3. Ion and electron trajectories. The top, middle, and bottom panels show, respectively, exploding ions, surrounding ions, and electrons. The thick solid and dotted lines indicate $x_{iEb}(t)$ and $x_{iSb}(t)$, respectively. The dash-dotted line in the bottom panel represents $x_{eb}(t)$.

estimate (35). Some ion trajectories near the ion overlapping region rapidly change their directions. This scattering begins shortly before v_{iEb} becomes zero for the first time. As a result, crossing of trajectories occurs even among the lines of exploding ions and among surrounding ions. This suggests that localized strong fields are generated. The bottom panel shows that the exploding electrons (solid lines) do not pass the surrounding electrons (dotted lines), indicating that they are not mixed. Their boundary x_{eb}, which is represented by the thick dashed-and-dotted line, is between x_{iSb} and x_{iEb} for $\Omega_{i0}t\lesssim 2$. After $\Omega_{i0}t\simeq 1$, on both sides of the boundary x_{eb}, we find regions where the trajectory lines are concentrated. These two regions gradually move away from each other. Ion trajectories are also concentrated in these regions. These are shock waves, one propagating forward in the surrounding plasma away from x_{eb} and the other backward in the exploding plasma.

Figure 4 displays phase spaces and field profiles at an early time $\Omega_{i0}t=0.2$: from top to bottom, p_{ixE} (momentum p_x of the exploding ions), p_{ixS} (p_x of the surrounding ions), p_y of the two kinds of ions, p_{exE}, p_{exS}, electron density (the number of electrons per cell), magnetic field B_z, and electric fields E_x and E_y. Electron phase space (x,p_y) is not shown here; it looks quite similar to (x,p_x) because the electron gyroperiod

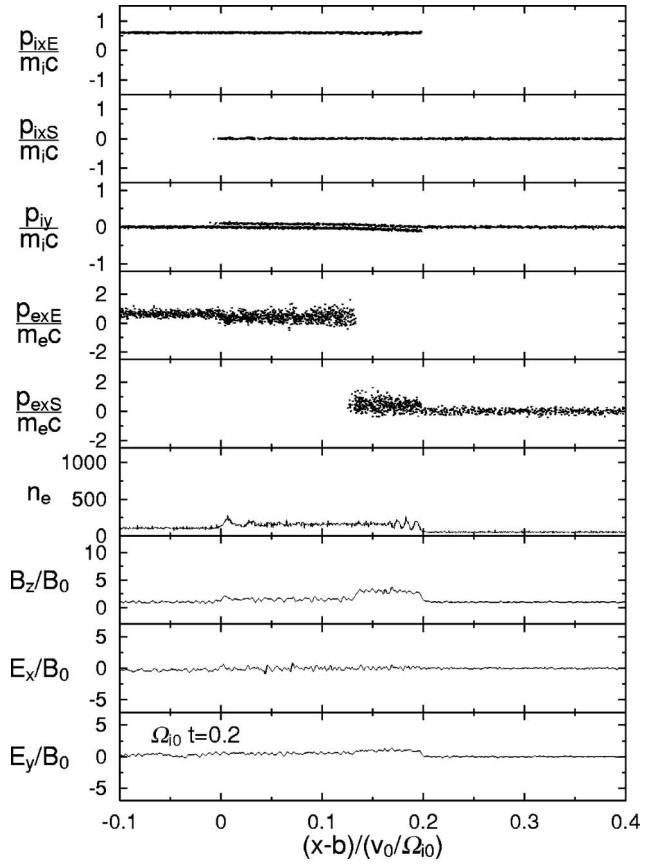

FIG. 4. Ion and electron phase spaces and field profiles at $\Omega_{i0}t=0.2$. Here, n_e is the number of electrons per cell.

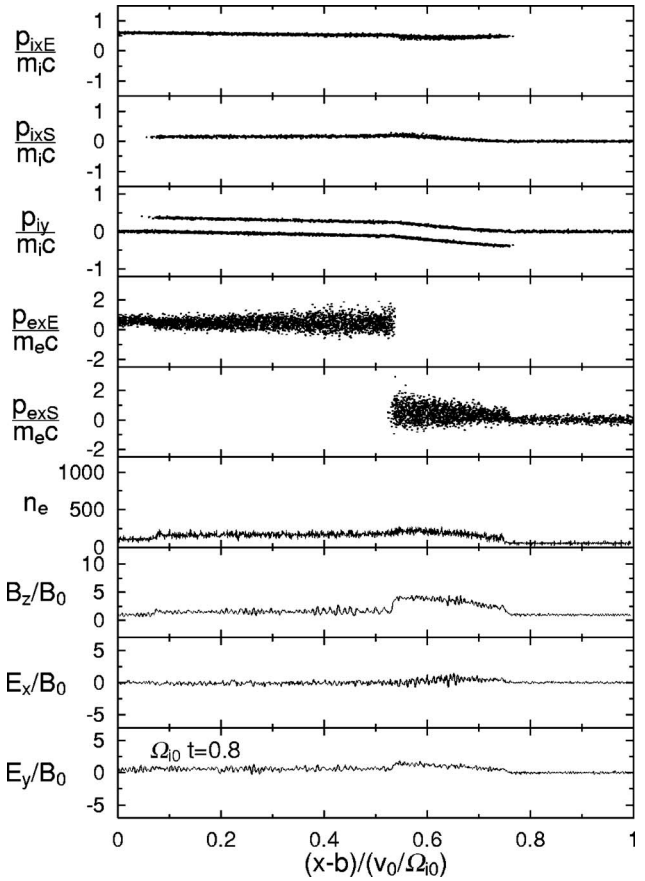

FIG. 5. Ion and electron phase spaces and field profiles at $\Omega_{i0}t=0.8$.

is short (p_x and p_y of the electrons, however, have different average values due to the $\boldsymbol{E}\times\boldsymbol{B}$ drift). Comparison of the top and second panels shows that the exploding ions have penetrated considerably deep in the region of the surrounding ions by this time, while the fourth and fifth panels indicate that the exploding and surrounding electrons are clearly separated at their boundary x_{eb} (the two kinds of electrons overlap in a narrow region of the order of the electron gyroradius). The magnetic field is intensified in the ion overlapping region. From the electron density profile (the ion density is not shown here because $n_i \simeq n_e$), we notice that some instabilities are growing near the left- and right-hand boundaries of the ion overlapping region (near x_{iSb} and near x_{iEb}). Except for these short-wavelength fluctuations, however, n_e is roughly constant in the ion overlapping region at this moment; n_{eS} has become approximately three times as high as that in the upstream region, n_{eS0}. Since $n_{eS0}=n_{eE0}/2$, this indicates that n_{eS} has been compressed more strongly than n_{eE}; i.e., $n_{eS}/n_{eS0}=2n_{eE}/n_{eE0}$ at this moment. The magnetic field is thus stronger in the front layer $x_{eb}<x<x_{iEb}$ than in $x_{iSb}<x<x_{eb}$.

Figures 5, 7, and 8 show the same quantities at later times; note, however, that the length scale is twice as large as that in Fig. 4. At $\Omega_{i0}t=0.8$ (Fig. 5), p_{ixE}'s are still much greater than p_{ixS}'s. They are, however, getting closer in the front layer. The p_{iyS}'s, which were nearly zero in Fig. 4, are growing faster than p_{ixS}'s and p_{iyE}'s, which is in accord with the theoretical prediction in Sec. II. The p_{ixE}'s are being converted to p_{iyE}'s. The conversion is particularly enhanced in the front layer. This is related to the fact that the magnetic field has become stronger there than in other regions; Eqs. (13) and (25) indicate that p_y's increase in magnitude more rapidly in a higher B_z in the early phase. In the density and field profiles, we still find short-wavelength fluctuations. Their amplitudes are, however, kept small. [The instability is thought to be caused by the cross-field relative velocities of the two kinds of ions and electrons. Because it does not play an important role in the development of the two plasmas, we do not go into details of the instability[32–37] (see the Appendix).]

Figure 6 shows the force on particles in the y direction at $\Omega_{i0}t=0.8$. [Each value, $F_y=(E_y-v_xB_z/c)/B_0$, is an average over particles in ten cells.] For the exploding ions (top left panel), these values are negative in the front layer $x_{eb}<x<x_{iEb}$, while they are closer to zero behind it. That is, the magnetic force exceeds the electric force in the front part; the conversion of v_x to v_y, therefore, occurs in a time scale of a gyroperiod. The two forces are, however, almost balanced in the region $x<x_{eb}$; consequently, the ions behind the front layer move nearly straight in the x direction, as was shown in Figs. 3–5. These different motions result in the compression of the exploding ions in the front part. It is interesting to note, however, that the forces on the surrounding ions are positive, particularly in the front layer (middle left panel); as a result, the forces that are averaged over all the ions are nearly zero in the entire region (bottom left panel). The right

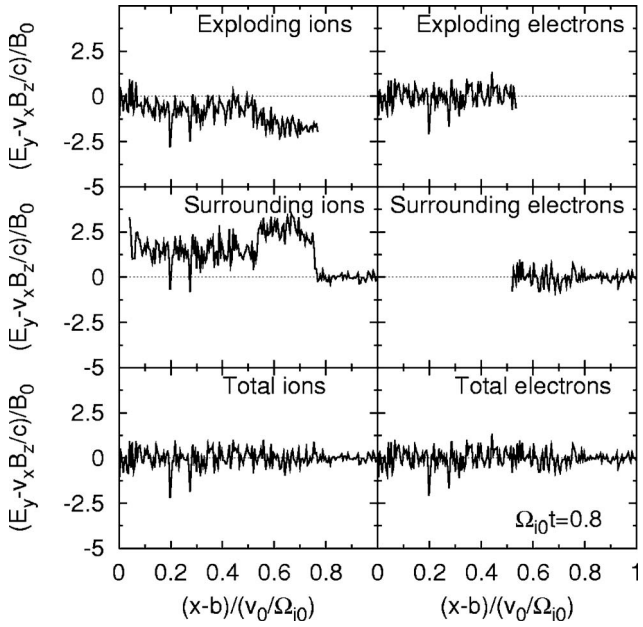

FIG. 6. Forces in the y direction at $\Omega_{i0}t=0.8$. For the exploding ions in the front layer ($x_{eb}<x<x_{iEb}$), the magnetic force dominates the electric force. At this moment, $(x_{eb}-b)/(v_0/\Omega_{i0})=0.53$.

panels show electrons. The forces are nearly zero at all the points for both the exploding and surrounding electrons, indicating that they move with the $\boldsymbol{E}\times\boldsymbol{B}$ drift.

In the field profiles at $\Omega_{i0}t=1.2$ (Fig. 7), we find two

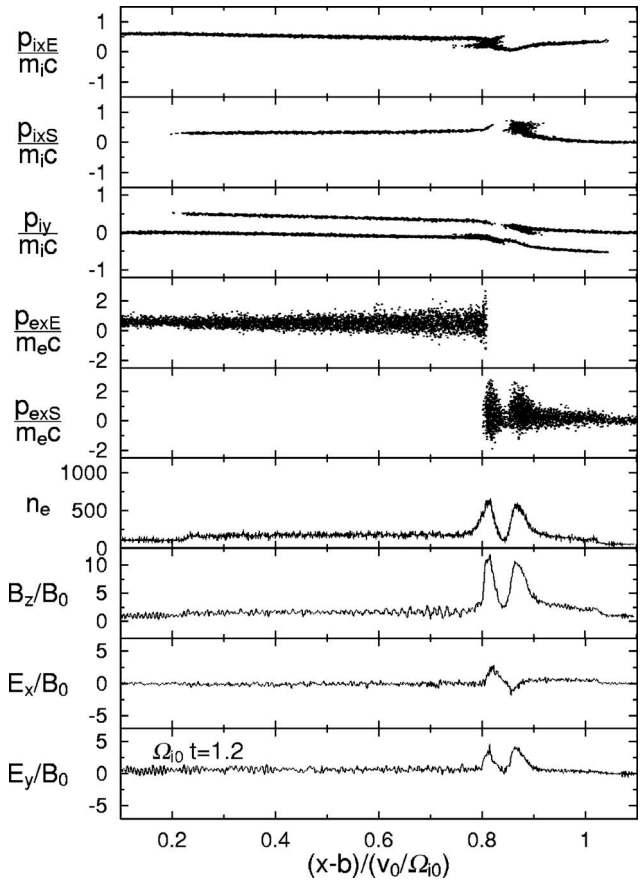

FIG. 7. Ion and electron phase spaces and field profiles at $\Omega_{i0}t=1.2$.

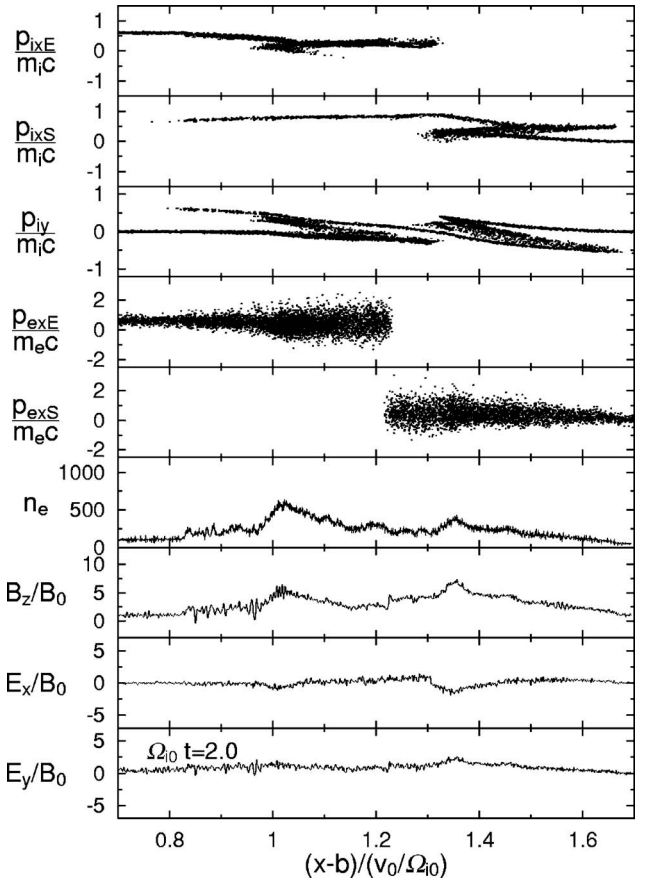

FIG. 8. Ion and electron phase spaces and field profiles at $\Omega_{i0}t=2.0$.

large peaks near x_{eb}. The left and right peaks mainly contain exploding and surrounding ions, respectively. Around these peaks, p_{ixE}'s and p_{ixS}'s are strongly deformed. The two peaks are formed because the rise in B_z in the front layer reflects the exploding ions backward (relative to the electrons there, in which the magnetic fields are frozen) and the surrounding ions forward; note that the ion and electron speeds were in the order $v_{ixS}<v_d<v_{ixE}$ before the reflection. Because of the reflection, the distribution functions are highly anisotropic near the two pulses. As Fig. 8 shows, the reflected particles eventually move to the downstream region owing to the magnetic force; as a result, the kinetic energy of random motions increases behind the pulses. (For the ion reflection by a shock wave, see Refs. 20 and 25–30. For shock simulations for a plasma containing positrons, see Ref. 31.) These two peaks propagate as magnetosonic pulses (compare Figs. 7 and 8). Their velocities from time $\Omega_{i0}t=1.2$ to 4.2 are $9.2v_{\rm ms}$ (right pulse) and $5.1v_{\rm ms}$ (left pulse). Their velocities relative to the electron boundary x_{eb}, whose velocity is $6.3v_{\rm ms}$, are $2.9v_{\rm ms}$ (right pulse) and $-1.2v_{\rm ms}$ (left pulse); the latter is therefore the reverse shock, moving back in the exploding plasma. The exploding and surrounding electrons are still clearly separated in the coordinate space.

Figure 9 shows the force on particles F_y at $\Omega_{i0}t=1.2$. In contrast to Fig. 6, the exploding ions have positive F_y's near the front layer, $0.8\lesssim(x-b)/(v_0/\Omega_{i0})\lesssim 0.9$. This is due to the reflected ions. In addition, instead of the exploding ions, the surrounding ions have negative F_y's near the front layer. In

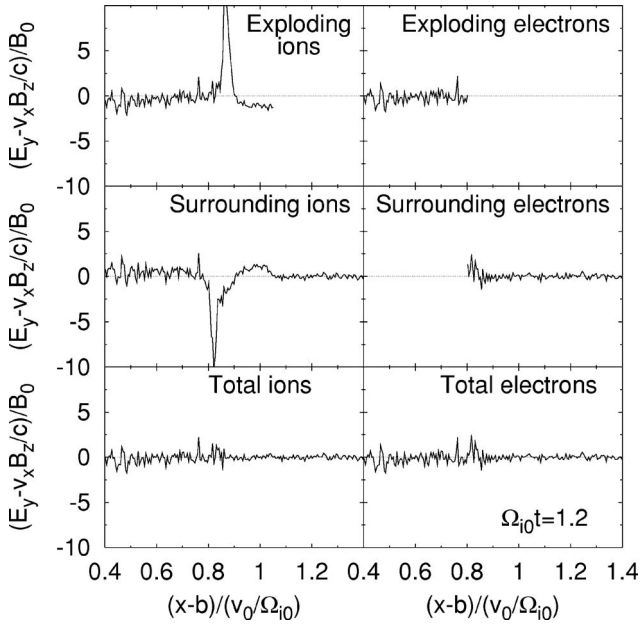

FIG. 9. Force F_y at $\Omega_{i0}t=1.2$. Surrounding ions in front of x_{eb} have negative F_y. At this moment, $(x_{eb}-b)/(v_0/\Omega_{i0})=0.8$.

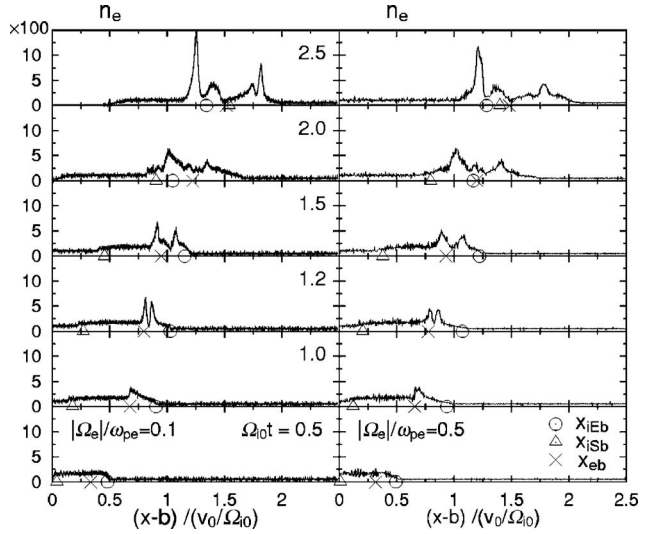

FIG. 10. Electron density profiles for $|\Omega_e|/\omega_{pe}=0.1$ (left panels) and for $|\Omega_e|/\omega_{pe}=0.5$ (right panels). The circles, triangles, and crosses, respectively, indicate the positions of x_{iEb}, x_{iSb}, and x_{eb}. The left and right panels show quite similar profiles at the same times.

this region, some surrounding ions have high v_x. These ions had once been overtaken by the exploding ions in the front layer and have passed them again. Their high v_x's are then converted to v_y's by the magnetic force. This explains the fact that in Fig. 3, many of the exploding ions continue to move nearly straight while some of the surrounding ions suffer a sharp decrease (and subsequent increase) in v_x after $\Omega_{i0}t \gtrsim 1.5$, like x_{iEb} in $1 \lesssim \Omega_{i0}t \lesssim 2.5$.

From Figs. 3–8, we have seen that around the time $\Omega_{i0}t=1$, x_{iEb} is considerably decelerated and the plasma and magnetic field are compressed in the front layer. Around this time, the collective effects suggested in Sec. II B appear, which are not included in the theoretical analysis in Sec. II A. Then, two magnetosonic pulses are generated near the front layer and move away.

Essentially the same phenomena have been observed in simulations with different field strengths and density ratios. Figure 10 compares the development of the density profile for the external magnetic field strength $|\Omega_e|/\omega_{pe}=0.1$ (left panels) and that for $|\Omega_e|/\omega_{pe}=0.5$ (right panels); other parameters, such as the initial densities and velocities, are the same. The circles, triangles, and crosses, respectively, indicate the positions of x_{iEb}, x_{iSb}, and x_{eb}. Even though the external magnetic field in the right panels is five times as strong as that in the left panels, the density profiles in the left and right panels at the same times are quite similar. Since the time and length are, respectively, scaled in units of Ω_{i0}^{-1} and v_0/Ω_{i0} in these panels, this indicates that the magnetic field plays a fundamental role in the formation of shock waves. Figure 11 also supports this; it shows density profiles for higher density ratios, $n_{iE0}/n_{iS0}=5$ (left panels) and $n_{iE0}/n_{iS0}=10$ (right panels). The strength of the external magnetic field is $|\Omega_e|/\omega_{pe}=0.1$, and other parameters are the same as those in the previous simulations. In both panels, we again find two large peaks at $\Omega_{i0}t=1.2$; one then propagates forward relative to the electrons and the other backward.

After the two pulses are generated at $\Omega_{i0}t \simeq 1$, the evolution of the density profile is rather complicated, owing to the complex motions of exploding and surrounding particles. In either left or right panels in Fig. 10, for instance, the amplitude of the backward pulse is especially large at $\Omega_{i0}t=2.5$. This is mainly related to the motion of the reflected exploding ions; ion reflection can cause amplitude oscillation of magnetosonic pulses.[28] This enhancement of the amplitude is therefore temporary, lasting for a period $\Omega_{i0}t \simeq 0.5$ in these cases. For the parameters of Fig. 11, this phenomenon occurs at $\Omega_{i0}t \simeq 4$, which is not shown here.

Finally, we mention the effect of the initial density ratio n_{iE0}/n_{iS0} on the width of the front layer, $\Delta_{fr}=x_{iEb}-x_{eb}$. Figure 12 shows the time variations of Δ_{fr} for various density ratios.

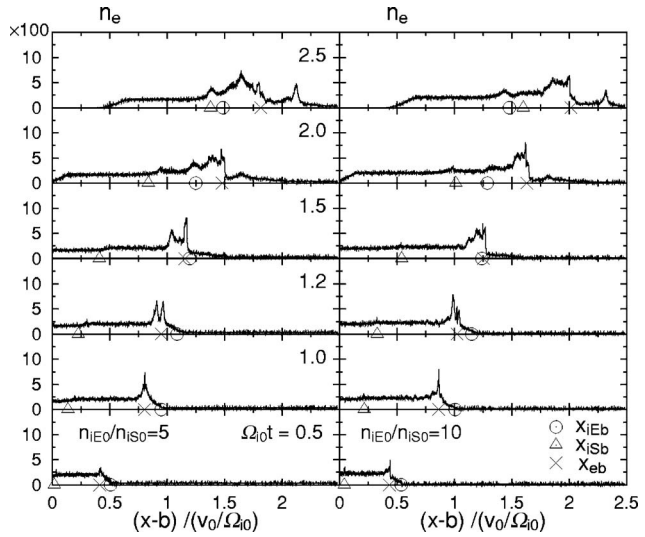

FIG. 11. Electron density profiles for the initial density ratio $n_{iE0}/n_{iS0}=5$ (left panels) and for $n_{iE0}/n_{iS0}=10$ (right panels).

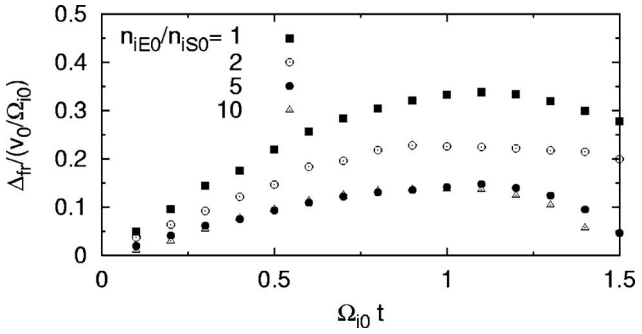

FIG. 12. Time variations of front-layer widths Δ_{fr}. The width decreases with increasing density ratio n_{iE0}/n_{iS0}.

Each width has its maximum value at $\Omega_{i0}t \simeq 1$. As expected from the discussion in Sec. II B, it decreases with increasing density ratio n_{iE0}/n_{iS0}. It seems, however, that there is a lower bound. The maximum values of Δ_{fr} for $n_{iE0}/n_{iS0}=5$ and 10 are nearly the same and are of the order of the gyroradius of thermal ions ρ_{iT}; $\Delta_{\mathrm{fr}}=0.14(v_0/\Omega_{i0})=2.7\rho_{iT}$.

It is noted that x_{iEb} is not necessarily the front of the exploding ions for $\Omega_{i0}t \gtrsim 1.5$ (see Fig. 3). Further, Figs. 10 and 11 show that x_{iEb} is overtaken by x_{eb}. The "front layer" defined as the region $x_{eb}<x<x_{iEb}$ disappears after producing the two pulses.

IV. SUMMARY

We have studied shock formation processes arising from the collision of two plasmas, which we called the exploding and surrounding plasmas, for the case in which the initial velocity of the exploding plasma, which is taken to be $\boldsymbol{v}_0=(v_0,0,0)$, is perpendicular to the external magnetic field, $\boldsymbol{B}_0=(0,0,B_{z0})$. We have assumed that v_0 is high and B_0 is weak so that the ion gyroradius v_0/Ω_i is much greater than the width of the shock transition region.

It is analytically shown that immediately after the penetration of the exploding plasma, the electric field E_y, which is induced by the cross-field plasma motion, accelerates the surrounding ions in the y direction (perpendicular to $\boldsymbol{v}_0$ and $\boldsymbol{B}_0$); their velocities are soon converted to v_x owing to the $\boldsymbol{v}\times\boldsymbol{B}$ force. The v_x of the exploding ions in the front layer goes down from v_0 also by the magnetic force; as a result, roughly a half gyroperiod after the penetration, the exploding ions in the front part are overtaken by the surrounding ions that were initially near the boundary. The electron motions are described with the $\boldsymbol{E}\times\boldsymbol{B}$ drift; hence, the exploding and surrounding electrons are not mixed. In the front layer of the exploding ions, the plasma and magnetic-field lines are compressed.

We have then verified these predictions with one-dimensional (one space coordinate and three velocities), electromagnetic particle simulations. Furthermore, they show that the intensified magnetic field in the front layer reflects the surrounding ions forward relative to the electrons and the exploding ions backward. This results in the generation of two large magnetosonic pulses propagating away from the front layer as forward and reverse shock waves. Up to the time of the formation of the two pulses, $\Omega_i t \sim 1$, the time scale is determined basically by the magnetic field, and the length scale by B_0 and v_0.

ACKNOWLEDGMENTS

This work was carried out by the joint research program of the Solar-Terrestrial Environment Laboratory, Nagoya University, and by the collaboration program, NIFS06KTAT017, of the National Institute for Fusion Science.

APPENDIX: INSTABILITIES DUE TO CROSS-FIELD ION MOTIONS

We discuss here instabilities that could grow in the ion overlapping region in the present simulations. The electron-electron two-stream instability should be unimportant in the present case because the electron kinetic energy corresponding to v_0 is m_e/m_i times as small as that of the ions. Further, the time and length scales in which two electron streams can exist are only of the order of the electron gyroperiod and gyroradius, respectively. We therefore consider instabilities due to cross-field ion motions.

In the 1970s, many authors studied instabilities caused by ion motions across a magnetic field to explain the experiments of turbulent heating.[32] Among them, the modified-two-stream instability was thought to be especially important;[33] one obtains its dispersion relation under the assumption that the ions are effectively unmagnetized while the electrons are magnetized.

The physical situations in the present simulations differ from those for the above instability in that we have two different ion groups and the wavenumber $\boldsymbol{k}$ is perpendicular to $\boldsymbol{B}$. As in the modified-two-stream instability, however, the length scale of the fluctuations observed in the early stage of the simulations is much shorter than the ion gyroradius. With calculations similar to those in Ref. 33, therefore, we obtain a dispersion relation for a system with two ion beams,

$$1+\frac{\omega_{pe}^2}{\Omega_e^2-\omega^2}-\frac{\omega_{pa}^2}{(\omega-kU_a)^2}-\frac{\omega_{pb}^2}{(\omega-kU_b)^2}=0, \tag{A1}$$

where the subscripts a and b denote two different ion groups. (To compare with the simulations in Sec. III, we interpret the two ion groups as the exploding and surrounding ions.)

Assuming that ω is given as $\omega=kU_b+i\gamma$ and that $\gamma^2 \ll k^2U_b^2$, we have approximate growth rates as

$$\gamma=\omega_{pb}\left(\frac{\omega_{pe}^2}{k^2U_b^2-\Omega_e^2}+\frac{\omega_{pa}^2}{k^2(U_a-U_b)^2}-1\right)^{-1/2}. \tag{A2}$$

We have growing waves if

$$\frac{\omega_{pe}^2}{k^2U_b^2-\Omega_e^2}+\frac{\omega_{pa}^2}{k^2(U_a-U_b)^2}>1. \tag{A3}$$

We will also have unstable waves of the form $\omega=kU_a+i\gamma$. If $\omega_{pa} \sim \omega_{pb}$, the growth rates of these two modes should be of the same order.

Figure 13 shows the time variation of a Fourier amplitude $n_k(t)$ of density perturbations for the simulation shown

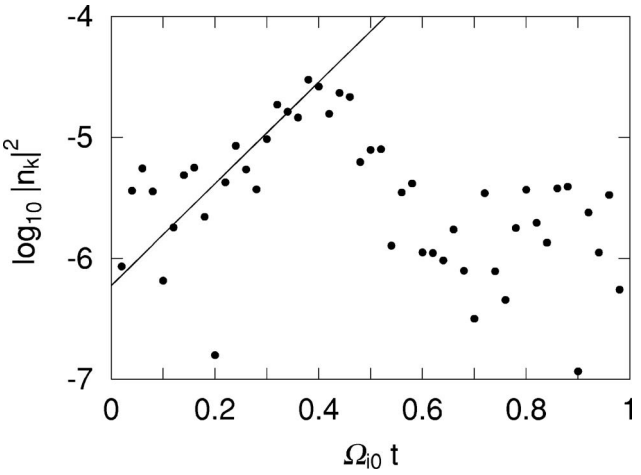

FIG. 13. Time variation of a Fourier amplitude of density perturbations. Here, the amplitude is normalized to that of the $k=0$ mode.

by Figs. 3–9. Here, the amplitude is normalized to that of $k=0$ mode. We have plotted $|n_k(t)|^2$ for the mode that had the longest growth time. Its wavenumber is $k\rho_{iT}=12$ and satisfies the condition (A3). In the early phase, $\Omega_{i0}t<0.4$, $|n_k(t)|^2$ increases nearly exponentially from the initial thermal level with a growth rate $\gamma=4.8\Omega_{i0}$. This value is 70% of the growth rate estimated from Eq. (A2) with $U_a=-U_b=v_0/2$, which are the values in the early stage in the rest frame of the electrons. We see that $|n_k(t)|^2$ grows to values approximately 50 times as large as its initial one. Around the time $\Omega_{i0}t=0.4$, it is saturated and then begins to decrease. This quick saturation would be due to the rapid change in the shape of the velocity distribution functions; i.e., the electron velocity distribution quickly spreads in the ion-overlapping region [the dispersion relation (A2) is based on a cold plasma model], and the relative velocity between the exploding and surrounding ions reduces.

Before closing this Appendix, we make a brief mention of the Weibel instability, which was first studied by Weibel in 1959.[34] He theoretically showed that transverse electromagnetic waves can grow in a plasma with anisotropic electron temperature. Recently, magnetic field generation due to electron counter streaming in electron-positron plasmas has attracted a great deal of attention in astrophysical plasmas.[35,36] These instabilities are also referred to as the Weibel instability. In addition, a similar subject has been studied in laser-produced electron-ion plasmas.[37] In these studies, electron flow is parallel to the external magnetic field (or there is no external magnetic field). Since we are concerned with cross-field plasma motions in the present paper, either the Weibel instability studied in the first paper[34] or that in recent ones[35–37] is unimportant. If we extend our study to high-speed, parallel counter streaming cases, however, those instabilities may become important.

[1] C. F. McKee and L. L. Cowie, Astrophys. J. **195**, 715 (1975).
[2] P. R. Woodward, Astrophys. J. **207**, 484 (1976).
[3] J. Nuckolls, Nature (London) **239**, 139 (1972).
[4] D. J. Forrest and E. L. Chupp, Nature (London) **305**, 291 (1983).
[5] H. Nakajima, T. Kosugi, K. Kai, and S. Enome, Nature (London) **305**, 292 (1983).
[6] A. Jeffrey and T. Taniuti, *Non-linear Wave Propagation* (Academic Press, New York, 1964).
[7] R. Z. Sagdeev, in *Reviews of Plasma Physics*, edited by M. A. Leontovich (Consultants Bureau, New York, 1966), Vol. 4, pp. 23–91; M. A. Lee, V. D. Shapiro, and R. Z. Sagdeev, J. Geophys. Res., [Solid Earth] **101**, 4777 (1996); V. D. Shapiro and D. Üçer, Planet. Space Sci. **51**, 665 (2003).
[8] Y. Ohsawa, Phys. Scr., T **107**, 32 (2004); M. Sato, S. Miyahara, and Y. Ohsawa, Phys. Plasmas **12**, 052308 (2005).
[9] K. Koyama, R. Petre, E. V. Gotthelf *et al.*, Nature (London) **378**, 255 (1995).
[10] T. Tanimori, Y. Hayami, S. Kamei *et al.*, Astrophys. J. Lett. **497**, L25 (1998).
[11] L. I. Sedov, *Similarity and Dimensional Methods in Mechanics* (Academic Press, New York, 1959).
[12] B. A. Remington, D. Arnett, R. P. Drake, and H. Takabe, Science **284**, 1488 (1999).
[13] D. W. Forslund and C. R. Shonk, Phys. Rev. Lett. **25**, 1699 (1970).
[14] L. Spitzer, *Physical Processes in the Interstellar Medium* (Wiley-Interscience, New York, 1978).
[15] J. H. Adlam and J. E. Allen, Philos. Mag., Suppl. **3**, 448 (1958).
[16] L. Davis, R. Lüst, and A. Schlüter, Z. Naturforsch. A **13**, 916 (1958).
[17] C. S. Gardner and G. K. Morikawa, Commun. Pure Appl. Math. **18**, 35 (1965).
[18] T. Kakutani, H. Ono, T. Taniuti, and C. C. Wei, J. Phys. Soc. Jpn. **24**, 1159 (1968).
[19] Y. Ohsawa, Phys. Fluids **29**, 1844 (1986); **29**, 2474 (1986).
[20] C. S. Morawetz, Phys. Fluids **4**, 988 (1961).
[21] D. A. Tidman and N. A. Krall, *Shock Waves in Collisionless Plasmas* (John Wiley & Sons, New York, 1971).
[22] R. Z. Sagdeev, in *Reviews of Plasma Physics*, edited by M. A. Leontovich (Consultants Bureau, New York, 1966), Vol. 4, pp. 23–91.
[23] R. J. Taylor, D. R. Baker, and H. Ikezi, Phys. Rev. Lett. **24**, 206 (1970).
[24] P. C. Liewer, A. T. Lin, J. M. Dawson, and M. Z. Caponi, Phys. Fluids **24**, 1364 (1981).
[25] D. Biskamp and H. Welter, Nucl. Fusion **12**, 663 (1972).
[26] C. F. Kennel and R. Pellat, J. Plasma Phys. **15**, 335 (1976).
[27] D. W. Forslund, K. B. Quest, J. U. Brackbill, and K. Lee, J. Geophys. Res. **89**, 2142 (1984).
[28] Y. Ohsawa, Phys. Fluids **28**, 2130 (1985); T. Kawashima, S. Miyahara, and Y. Ohsawa, J. Phys. Soc. Jpn. **72**, 1664 (2003).
[29] B. Lembege and J. M. Dawson, Phys. Fluids B **1**, 1001 (1989).
[30] R. L. Tokar, S. P. Gary, and K. B. Quest, Phys. Fluids **30**, 2569 (1987).
[31] M. Hoshino, J. Arons, Y. A. Gallant, and B. Langdon, Astrophys. J. **390**, 454 (1992); H. Hasegawa, K. Kato, and Y. Ohsawa, Phys. Plasmas **12**, 082306 (2005).
[32] N. Krall and P. Liewer, Phys. Rev. A **4**, 2094 (1971).
[33] E. Ott, J. B. McBride, J. H. Orens, and J. P. Boris, Phys. Rev. Lett. **28**, 88 (1972).
[34] E. S. Weibel, Phys. Rev. Lett. **2**, 83 (1959).
[35] Y. Kazimura, J. I. Sakai, T. Neubert, and S. V. Bulanov, Astrophys. J. Lett. **498**, L183 (1998).
[36] T. Piran, Phys. Rep. **333–334**, 529 (2000).
[37] E. M. Epperlein and A. B. Bell, Plasma Phys. Controlled Fusion **29**, 85 (1987).